

## Diagnosing the Neutral Interstellar Gas Flow at 1 AU with IBEX-Lo

E. Möbius · H. Kucharek · G. Clark · M. O'Neill · L. Petersen · M. Bzowski · L. Saul ·  
P. Wurz · S.A. Fuselier · V.V. Izmodenov · D.J. McComas · H.R. Müller ·  
D.B. Alexashov

Received: 17 September 2008 / Accepted: 16 March 2009 / Published online: 22 April 2009  
© Springer Science+Business Media B.V. 2009

**Abstract** Every year in fall and spring the Interstellar Boundary Explorer (IBEX) will observe directly the interstellar gas flow at 1 AU over periods of several months. The IBEX-Lo sensor employs a powerful triple time-of-flight mass spectrometer. It can distinguish and image the O and He flow distributions in the northern fall and spring, making use of sensor viewing perpendicular to the Sun-pointing spin axis. To effectively image the narrow flow distributions IBEX-Lo has a high angular resolution quadrant in its collimator. This quadrant is employed selectively for the interstellar gas flow viewing in the spring by electrostatically shutting off the remainder of the aperture. The operational scenarios, the expected data,

---

E. Möbius (✉) · H. Kucharek · G. Clark · M. O'Neill · L. Petersen  
Space Science Center & Department of Physics, University of New Hampshire, Durham, NH 03824,  
USA  
e-mail: [Eberhard.Moebius@unh.edu](mailto:Eberhard.Moebius@unh.edu)

M. Bzowski  
Space Research Centre, Polish Academy of Sciences, Warsaw, Poland

L. Saul · P. Wurz  
Physikalisches Institut, Universität Bern, 3012 Bern, Switzerland

S.A. Fuselier  
Lockheed Martin Advanced Technology Lab, Palo Alto, CA, USA

V.V. Izmodenov  
Moscow State University and Space Research Institute, Russian Academy of Sciences, Moscow, Russia

D.J. McComas  
Southwest Research Institute, San Antonio, TX, USA

H.R. Müller  
Department of Physics and Astronomy, Dartmouth College, Hanover, NH, USA

D.B. Alexashov  
Space Research Institute (IKI) and Institute for Problems in Mechanics, Russian Academy of Sciences,  
Moscow, Russia

and the necessary modeling to extract the interstellar parameters and the conditions in the heliospheric boundary are described.

The combination of two key interstellar species will facilitate a direct comparison of the pristine interstellar flow, represented by He, which has not been altered in the heliospheric boundary region, with a flow that is processed in the outer heliosheath, represented by O. The O flow distribution consists of a depleted pristine component and decelerated and heated neutrals. Extracting the latter so-called secondary component of interstellar neutrals will provide quantitative constraints for several important parameters of the heliosheath interaction in current global heliospheric models. Finding the fraction and width of the secondary component yields an independent value for the global filtration factor of species, such as O and H. Thus far filtration can only be inferred, barring observations in the local interstellar cloud proper. The direction of the secondary component will provide independent information on the interstellar magnetic field strength and orientation, which has been inferred from SOHO SWAN Ly- $\alpha$  backscattering observations and the two Voyager crossings of the termination shock.

**Keywords** Interstellar gas · Heliosphere · Instrumentation

## 1 Introduction and Context

The local galactic environment of the Sun consists of a warm, relatively dilute, partially ionized, and quite structured interstellar gas cloud (e.g. reviews by Cox and Reynolds 1987; Frisch 1995). Apparently, the Sun finds itself close to a cloud boundary, possibly with a significant gradient in the ionization fraction of He (e.g. Cheng and Bruhweiler 1990; Wolff et al. 1999; Slavin and Frisch 2002). The environment and structure of the local interstellar cloud, including integral densities and relative speeds, has been studied on scales of several parsec through UV line absorption by the surrounding medium in the light of nearby stars (e.g. McClintock et al. 1978; Frisch 1981; Crutcher 1982; Lallement and Bertin 1992; Linsky et al. 1993). In a recent workshop “From the Heliosphere to the Local Bubble” at the International Space Science Institute in Bern, Switzerland, the heliosphere and its surroundings have been discussed in the context of their more extended environment of the Local Bubble (Möbius 2009, and references therein). It was also suggested in a consensus decision to call the interstellar medium immediately outside the heliosphere “Circum-Heliospheric InterStellar Medium (CHISM)”, which we use henceforth. The influence of the interstellar gas reaches deep into the heliosphere, for example, with the generation of pickup ions (e.g. Möbius et al. 1985; Gloeckler and Geiss 1998) and of anomalous cosmic rays (e.g. Klecker 1995; Jokipii 1998) as well as a slow down of the solar wind (Richardson et al. 1995).

The conditions in the surrounding interstellar medium and their consequences have changed dramatically over the history of the solar system (for a recent comprehensive compilation see Frisch 2006). In particular, the inventory of neutral interstellar gas, its spatial distribution, and its products in the inner heliosphere change substantially with external conditions, as does the filtering at the interface (Möbius et al. 2006; Müller and Zank 2004; Zank et al. 2006). Within the hot and very dilute plasma of the Local Bubble the heliosphere is moving through a succession of warm clouds that are similar to the one it is in currently. In fact, the heliosphere may be at the edge of one cloud while in transition to another (Redfield 2008).

The flow of several neutral gas species through the inner solar system is a very important tool for detailed diagnostics of the local cloud conditions. In this paper we will discuss how

the Interstellar Boundary Explorer (IBEX, McComas et al. 2009, [this issue](#)) will further this toolset by observing simultaneously at least interstellar oxygen and helium at two different locations in the Earth's orbit. We will begin by laying out the current knowledge and important questions that arose from recent observations, followed by an overview of neutral gas measurements of the interstellar flow, how modeling has to be combined with observations, and some anticipated results. Section 4 will contain a discussion of the IBEX capabilities in terms of the mission design and the instrumentation, followed by the planning of the interstellar flow observation campaigns in Sect. 5, and some conclusions with a look to the future.

## 2 Current Knowledge of the CHISM and Its Interaction with the Heliosphere

Together with the strength and variations of the solar wind, the very local conditions in the CHISM control the size and shape of the heliosphere. They also are responsible for the processes that control the heliospheric boundary regions. The basic understanding of the heliosphere and its interaction with the interstellar medium has been summarized in early reviews (Axford 1972; Fahr 1974; Holzer 1977; Thomas 1978). Since then substantial progress has been made in the global heliospheric modeling (e.g. Baranov and Malama 1993; Pauls et al. 1995; Zank et al. 1996; Linde et al. 1998; Fahr et al. 2000; Zank and Müller 2003; Malama et al. 2006; Izmodenov et al. 2008; and reviews by Zank 1999; Izmodenov and Kallenbach 2006). However, fixing the parameters in these models requires detailed knowledge of the very local boundary conditions. In a concurrent contribution Frisch et al. (2009, [this issue](#)) describe in detail the current knowledge of the interstellar medium that surrounds the heliosphere and how this information has been gathered. Therefore, we will only discuss the observations of interstellar neutrals inside the heliosphere here and how they pertain to the task at hand, i.e. the direct observation of neutral gas velocity distributions from a 1 AU vantage point.

Interstellar neutral gas penetrates into the inner heliosphere as a wind due to the relative motion between the Sun and the local interstellar medium. Through the interplay between this wind, the ionization of the neutrals upon their approach to the Sun, and the Sun's gravitational field (distinctly modified by radiation pressure for low energy H) a characteristic flow pattern and density structure is formed with a cavity close to the Sun and gravitational focusing on the downwind side (for all species except H). Starting with the analysis of backscattered solar Lyman  $\alpha$  intensity sky maps (Bertaux and Blamont 1971; Thomas and Krassa 1971), the parameters of H became accessible to observations. Using high-resolution line profiles of Ly- $\alpha$  with the Copernicus spacecraft, Adams and Frisch (1977) obtained first reasonable values for the H bulk speed and constrained its temperature. This method to determine the kinetic H parameters was substantially improved with the use of hydrogen absorption cells (Bertaux et al. 1985). Through the gravitational focusing of the interstellar He flow on the downwind side of the Sun, maps of the backscattered solar He I line at 58.4 nm that became available a few years after the H observations (Weller and Meier 1974) were used to obtain the bulk flow velocity vector, density, and temperature of He (see also Fahr et al. 1978; Wu and Judge 1979). Chassefière et al. (1986) compiled a critical evaluation of all interstellar density measurements, with values for  $n_{\text{H}}$  from 0.02 to 0.068  $\text{cm}^{-3}$ , including their latest value of  $0.065 \pm 0.01$ , and  $n_{\text{He}}$  from 0.0035 to 0.032  $\text{cm}^{-3}$ , including theirs of  $0.01 \pm 0.0045$ . Puzzling at that time was a counterintuitive difference between H and He in temperature, or depending on the parameter choice in their speed.

The discovery of interstellar He pickup ions at 1 AU (Möbius et al. 1985) introduced a first in-situ method for probing interstellar gas. This enabled an independent determination

of the interstellar He flow parameters (Möbius et al. 1995), but the method was hampered in its accuracy by strong variations in pickup ion fluxes (Möbius et al. 1998a) and the discontinuous data set of an Earth orbiting spacecraft. Continuous coverage in interplanetary space out to 5.4 AU and access to H<sup>+</sup> and He<sup>2+</sup> pickup ions with Ulysses SWICS provided a more precise determination of the H ( $0.11 \text{ cm}^{-3}$ ) and He ( $0.015 \text{ cm}^{-3}$ ) densities referenced to the termination shock (Gloeckler et al. 1997), and a more direct evaluation of the abundance of minor species, such as N, O and Ne, (Gloeckler and Geiss 2001) than had been obtained through anomalous cosmic rays (Cummings et al. 2002). Finally, direct observations of the neutral gas velocity distribution (Witte et al. 1996) have become available for He, with the most complete information on this key CHISM species yet.

Combining the aforementioned three in-situ observation methods for interstellar He and adding new observations of the relevant ionization rates in the inner heliosphere, Möbius et al. (2004) consolidated the physical parameters known for He from the CHISM, with consensus values of  $n_{\text{He}} = 0.015 \pm 0.002 \text{ cm}^{-3}$ ,  $v_{\text{He}} = 26.3 \pm 0.4 \text{ km/s}$ , and  $T_{\text{He}} = 6300 \pm 390 \text{ K}$ . A benchmark set of parameters of the CHISM proper was established because the heliosphere is essentially transparent for He. It became also quite clear that the direct neutral imaging observations provided by Ulysses GAS (Witte 2004) contributed with unambiguous and most detailed information about the kinetics of the CHISM and its flow through the heliosphere. This achievement leaves the total H density, the ionization environment coupled with the filtration of species that show a much stronger charge exchange interaction with the protons of the surrounding interstellar plasma, and the interstellar magnetic field to be determined.

The observation of H pickup ions (Gloeckler and Geiss 2001; Bzowski et al. 2008) and of the solar wind slowdown due to massloading with implanted interstellar H pickup ions (Richardson et al. 2008) provide the means to determine the neutral H density at the termination shock, while still leaving the neutral density in the CHISM up to modeling. Recently, both Voyager spacecraft have reached the termination shock. These observations constrain the overall size of the heliosphere and thus the CHISM pressure in the ram direction of the heliosphere. They also place strong constraints on the neutral and ion density of the surrounding interstellar medium (Izmodenov et al. 2004).

For the typical plasma densities in the surrounding interstellar cloud the mean free path for charge exchange of He exceeds several 1000 AU. The comparable number for H and O is of the order of 200 AU, i.e. comparable to the size of the heliosphere. Therefore, H and O, as well as a number of other species are subject to a substantial filtration between the pristine CHISM and the inner heliosphere (for reviews see Zank 1999; Müller and Zank 2004; Izmodenov et al. 2004; Izmodenov 2007). A noticeable fraction of the original neutral gas density of these species becomes part of the interstellar plasma that is forced to flow around the heliosphere, and thus the observed particle distribution of these species is depleted in the inner heliosphere. This is the definition of filtration. In turn, some of the ions of the outer heliosheath are converted into neutral atoms, a fraction of which has velocity vectors that bring them into the inner heliosphere. These atoms retain the velocity distribution of the outer heliosheath with a higher temperature than the original interstellar neutrals and a slower bulk velocity towards the inner heliosphere. This new distribution of neutrals is referred to as secondary neutrals. It has a distinctly different velocity distribution from the primary neutral gas population. A measurement of the velocity distribution function of all incoming neutrals (e.g., with a technique employed by Ulysses GAS) will provide much more direct diagnostics of the filtration than inferring the depletion factor from combined modeling of the neutral and ion densities inside and outside the heliosphere. Of course, this is true only if both the primary and secondary components can be identified in the combined velocity distribution.

The kinematics of the interstellar neutrals, including their secondaries, also carries the imprint of the interstellar magnetic field in the CHISM. Observations of an offset of the flow direction of interstellar H relative to that of the pristine He (Lallement et al. 2005) have provided insight into the direction and strength of the interstellar magnetic field (Izmodenov et al. 2005). In addition, the Voyager encounters with the termination shock have provided evidence of a distinct asymmetry of the heliosphere, which has also been interpreted as a specific tilt direction of the interstellar magnetic field, which appears to be consistent with what can be derived from the H flow observations (Izmodenov et al. 2005; Opher et al. 2006; Pogorelov et al. 2008). However, the direction determination still contains large uncertainties, and many questions about the strength of the influence of neutrals on the resulting deflection in the necessary global modeling remain (Pogorelov et al. 2006). Furthermore, the heliosphere is a rather dynamic entity, and temporal variations of the solar wind alter the location of the boundary structures in time and space, thus injecting into the observed asymmetry of the termination shock through the two consecutive encounters with the two Voyager spacecraft an additional uncertainty. Although the combined temporal and spatial variations of the shock location in an asymmetric heliosphere in three dimensions have been addressed in some of the global modeling attempts (Washimi et al. 2007; Izmodenov et al. 2008), the combined ambiguities cannot be resolved based on just the two Voyager observations.

Therefore, direct observations of the interstellar flow distribution of a species that is affected by the heliospheric interface will be key to resolving these issues. IBEX will provide observations of O, which will be complementary to the available information from the H backscattering measurements because the strength of the interaction and the kinematics of O are quite different since O is a minor constituent and has a much larger mass than H. Furthermore, this will be yet another independent measurement of the heliospheric asymmetry with a different technique. Also, IBEX will provide such data over the course of several years (in particular if the mission can be successfully extended beyond the primary mission of two years) so that uncertainties arising from temporal variations can be separated.

### 3 Direct Neutral Gas Observations and Their Inferences

As discussed above, the least model-dependent and most detailed information about the interstellar neutral gas flow through the heliosphere can be obtained from observations of the velocity distribution of the neutral gas under investigation close to the Sun. Keplerian trajectories provide a unique transformation of the original velocity distribution, after the passage through the heliospheric boundary, into an angular distribution as viewed by sensors between 1 and 2 AU from the Sun. After inclusion of all pertinent effects along the neutral trajectories, such as ionization and deflection by the Sun's gravitation and radiation pressure, the distribution at the boundary can be constructed from observations of directional maps of the flow at the peak energy of each species.

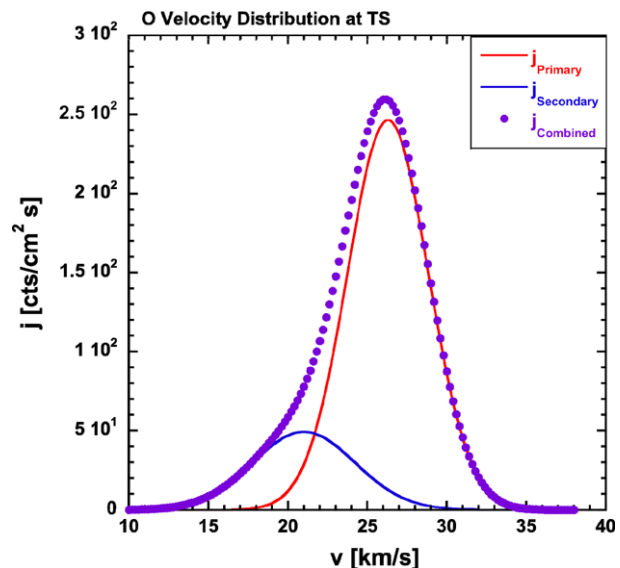
This enabling characteristic of the Sun's influence is very important because current observation methods for neutral atoms can provide precise angular images of the flow, but do not retain adequate energy resolution. This is true for the observation of interstellar helium through sputtering off a lithium-fluoride (LiF) surface as used in the Ulysses GAS instrument (Witte et al. 1996) and for negative ion conversion instruments for species, such as O and H (Fuselier et al. 2009, [this issue](#)). Therefore, the differential deflection of the interstellar neutral gas flow in the gravitational field of the Sun is utilized to convert speed differentials into an angular image. The analysis of such images through a deconvolution technique

has been described in detail by Banaszkiewicz et al. (1996). The very precise temperature and bulk flow values for CHISM He have been derived in this way (Witte 2004).

If the velocity distribution of H and O were studied with the same scrutiny, this would return decisive information about the filtration of these CHISM components, which is needed to derive exact neutral densities and the ionization-state of the CHISM. We will start the discussion with the velocity distribution of interstellar neutrals as they enter the heliosphere at the termination shock after having penetrated the boundary regions. This distribution contains unique information about the related processes, because filtration is accompanied by an effective slowdown and heating of the gases compared with their original state (Izmodenov et al. 1997), and about any deflection of the plasma due to the symmetry breaking role of the interstellar magnetic field (Izmodenov et al. 2005; Opher et al. 2006; Pogorelov et al. 2008). In detail, neutrals are first lost to the plasma flow by charge exchange and now contribute to a rather hot plasma distribution that is diverted around the heliosphere. In turn ions of this hot flow are converted to neutrals, of which a good fraction is directed towards the inner heliosphere. These neutrals constitute an additional secondary and rather hot gas distribution that is added to the original depleted flow. Because the fraction of these secondaries and their distribution scale with the column density of the ions in the outer heliosheath, the observation of the secondary neutral distribution holds a key to understanding the filtration processes in these regions and to constraining the overall geometry.

To estimate the observable effect and to define the parameters of the needed instrumentation we have simulated the neutral O distribution in the inner heliosphere and the respective observations at various positions of a spacecraft. It was assumed that the original O distribution in the CHISM resembles that of He with  $v_{\text{Bulk}} = 26.3$  km/s and  $T = 6400$  K as obtained by Witte (2004). According to Izmodenov et al. (1997), the filtration was adjusted so that the resulting neutral gas flow contains 50% of the primary distribution. Twenty percent of a secondary distribution with a reduced speed of  $v_{\text{Sec}} = 21$  km/s and  $T_{\text{Sec}} = 10000$  K were added. Figure 1 shows such a simulated velocity distribution of interstellar O as it enters the heliosphere at the termination shock. It is seen that the resulting distribution is asymmetric, with a substantial contribution from the secondary component on the low velocity side of

**Fig. 1** Simulated velocity distribution of the interstellar O-flow, as it enters the heliosphere at the termination shock. In addition to the primary O component with velocity and temperature as obtained for CHISM He, a secondary component of 20% of the overall distribution is added, produced by charge exchange in the heliospheric interface according to Izmodenov et al. (1997)



the distribution. If the distribution of the primary component is known, for example, from a simultaneous measurement of the He flow distribution, which resembles the pristine interstellar flow, then the secondary component can be reconstructed. In addition, a deviation of the flow vector direction from the original He CHISM flow for any species that are affected by the interface will also provide constraints on the local interstellar magnetic field.

To illustrate the combination of these effects, Fig. 2 shows the density distributions of neutral H and O. These distributions are normalized to the respective density values in the CHISM and are shown in a color-coded representation in a heliospheric cut that contains the interstellar magnetic field vector. Shown are the results from a global heliospheric simulation performed with a 3D kinetic magnetohydrodynamics model by the Moscow simulation group. For the simulations shown here, an interstellar magnetic field strength of 4.4  $\mu\text{G}$  (a somewhat higher field strength than favored previously) and a direction that is inclined by  $20^\circ$  relative to the interstellar flow vector have been adopted. This parameter set produces an approximately 10 AU difference in the distance of the termination shock from the Sun for the times and locations of the Voyager 1 and 2 crossings, as actually observed (Izmodenov et al. 2008). Because at least part of the observed termination shock distance difference could also be attributed to asymmetries arising from the interplanetary magnetic field configuration and to dynamic variations of the solar wind (Pogorelov et al. 2006; Washimi et al. 2007) it is important to note that other important observables result from this asymmetry that will be captured by IBEX.

Both the H and the O densities increase over their respective values in the CHISM when approaching the heliopause. The production of a slow secondary neutral component from the interstellar plasma that is forced to divert around the heliosphere overcompensates the loss of primary H and O from the original interstellar flow. Due to the inclined interstellar magnetic field the shapes of the heliospheric boundaries and the H and O wall are strongly asymmetric. A result of this asymmetry is a change in the direction of the mean velocity of the neutral atoms, which is imprinted on the secondary components of H and O. Comparing these predicted flow directions directly with observed interstellar neutral flow observations using IBEX-Lo will enable us to eliminate the persisting ambiguities in the evaluation of the Voyager asymmetry observations. The upper panel of Fig. 3 shows the flow deflection angles for interstellar H and O. For O the results are also broken out into the primary and secondary component. The overall deflection of H and O is that of the weighted combination of both components. The deflection of the combined O flow close to the Sun is still  $1.2^\circ$ , i.e. approximately half the deflection of H. Using predicted IBEX-Lo observations, it will be demonstrated below that both the overall deflection and the secondary component will be well visible and can be compared directly with interstellar He. The lower panel of Fig. 3 shows the normalized total number densities of neutral H and O as a function of distance from the Sun for the four cardinal directions within the plane that contains the interstellar magnetic field. The density increase in the H and O wall outside the heliopause is obvious for the upwind and side-wind directions. The depletion in the downwind direction is less prominent for O than for H. At 1 AU, where the observations with IBEX will be performed, the density of O is down to  $\approx 7\%$  of the CHISM value in the  $+$  and  $-90^\circ$  locations, which leads to neutral atom fluxes that are comfortably in IBEX-Lo's sensitivity range.

It should be noted that the filtration level and the resulting ratio of the primary and secondary components, which represents an observable quantity for O with IBEX-Lo, depend on the local ionization state of the CHISM. These parameters have been studied for H, O, and N by Izmodenov et al. (2004). In another sensitivity study, Müller and Zank (2004) modeled the processing of interstellar O and  $\text{O}^+$  against three different hydrogen backgrounds. The primary O is depleted while passing through the various heliospheric regions.

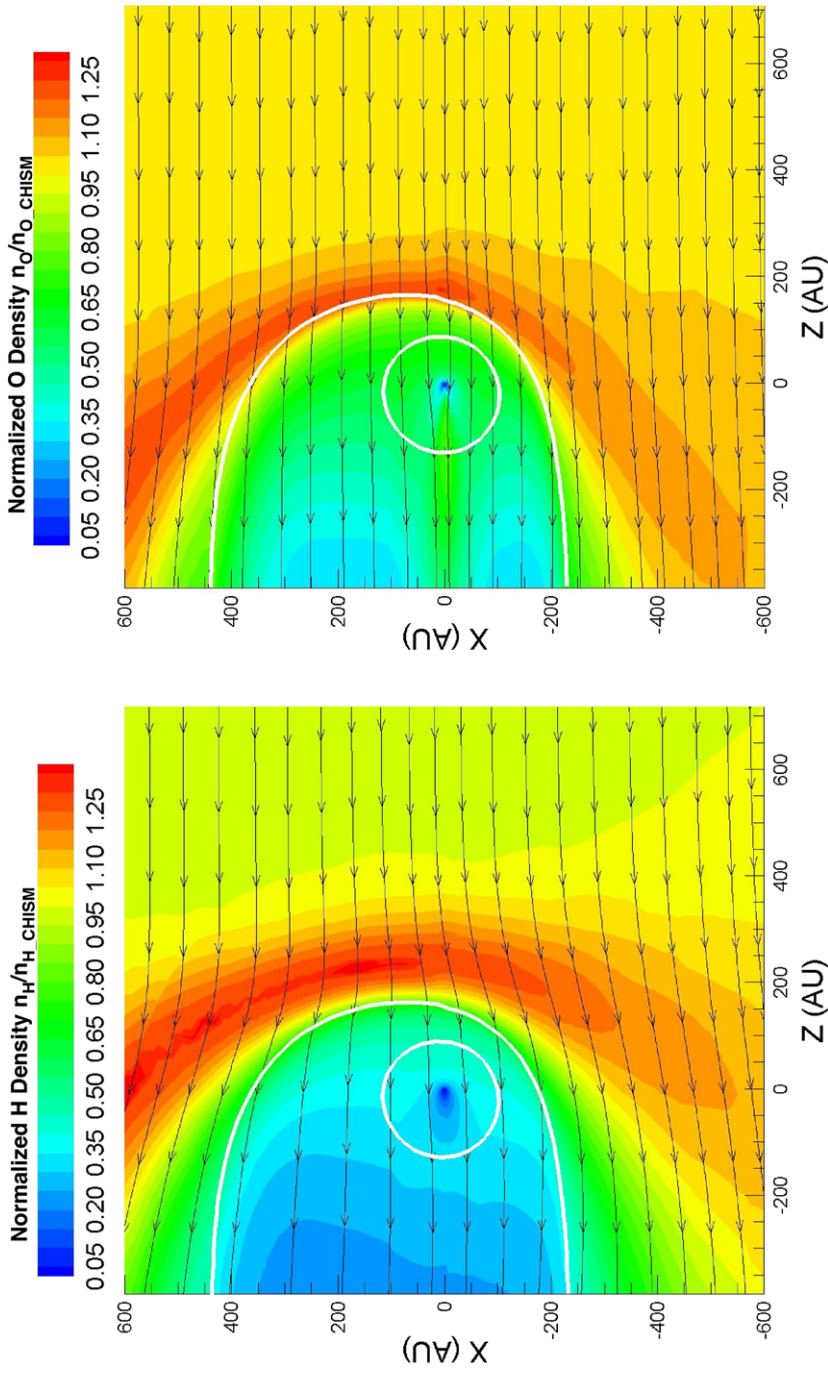


**Fig. 2** Color-coded representation of the H (left) and O (right) densities  $n_H/n_{H\_CHISM}$  and  $n_O/n_{O\_CHISM}$  in a heliospheric cut that contains the interstellar magnetic field vector ( $B = 4.4 \mu\text{G}$ , vector  $20^\circ$  relative to the CHISM flow vector)

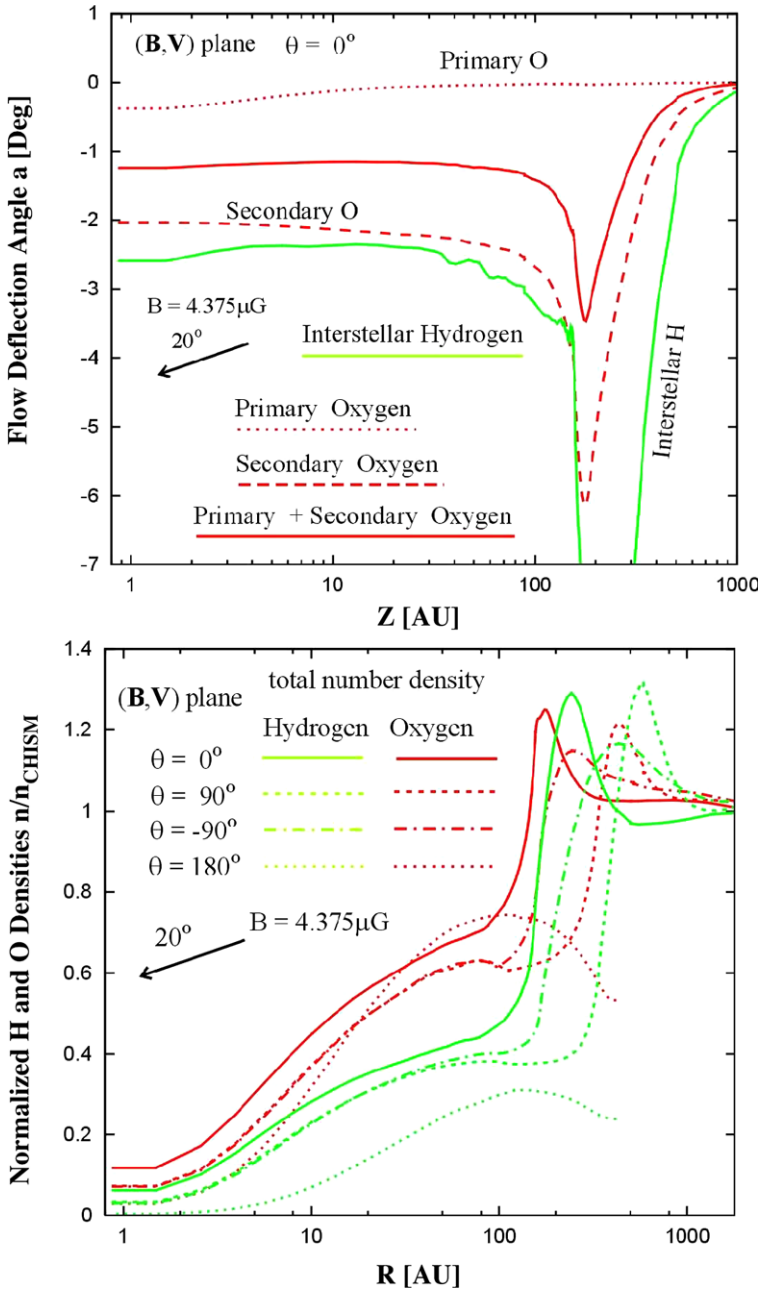


**Fig. 3** Deflection of the neutral gas flow from the original CHISM flow as a function of distance from the Sun along the inflow direction (*upper panel*) and normalized neutral densities as a function of radial distance from the Sun for four directions (*lower panel*). Shown are weighted combinations of the primary and secondary components for H and O. For the O flow directions in the *upper panel* also the primary and secondary component are shown separately

However, a substantial amount of secondary O is generated, especially when interstellar O<sup>+</sup> encounters the hydrogen wall. Because of the lower speeds upwind of the heliopause, characteristic mean-free-paths for charge exchange are quite low in this region, in the range of 10–100 AU. At the termination shock, the combined primary and secondary neutrals reach densities comparable or even exceeding the pristine neutral O CHISM density. This result was shown to be relatively insensitive to the different hydrogen backgrounds, which represented a range of hydrogen filtration values (Müller and Zank 2004). This interplay between O neutrals and ions with the hydrogen in the inner and outer heliosheath, which in turn depends on the strength of the interstellar bow shock (Müller et al. 2008), deserves further detailed study. In comparison with IBEX observations such simulations may therefore place important constraints on the existence and parameters of a heliospheric bow shock.

In the inner heliosphere, i.e. at <2 AU, the Sun's gravitational field can be employed to deduce flow velocities, from the observed image of the flow in the sky, at locations downstream of the Sun in the spring and fall of each year. A comparison of the He and O flow characteristics in the inner heliosphere will provide a powerful tool to deduce the amount of filtration and its related processes quantitatively from observations in the inner heliosphere. To turn the velocity distributions at large distances in a quantitative way into the angular distributions observed at 1 AU, the velocity distributions are handed over to the ray tracing program developed by the group at the Space Research Centre in Warsaw. This ray tracing of individual atoms includes all relevant effects, such as the Sun's gravitation and radiation pressure, as well as ionization on the way (Bzowski 2008).

Ideally one would also like to obtain the flow pattern of H in the inner heliosphere, which is being observed indirectly through Ly  $\alpha$  backscattering (Quémerais et al. 1999; Lallement et al. 2005). While IBEX-Lo is also sensitive to interstellar H in the ram direction at the low end of the sensor energy range, H is very strongly affected by radiation pressure so that predictions for its observation are rather uncertain. In turn, imaging neutral H from various locations may provide the most accurate account of this effect and will allow unambiguous separation of interface and radiation pressure related effects. In addition, radiation pressure may also serve as a discriminator between H and D, because the strength of the effect depends on the particle mass. As a result the D image will be separated from the H image in angle, thus giving a neutral imaging mass spectrograph an advantage in the observation of D in the CHISM. The D/H ratio in the interstellar medium has been considered an important data point for the evolution of matter (Linsky 1998; Mullan and Linsky 1998; Prantzos 1998) because D is the only isotope that is clearly being depleted by reactions inside stars over the primordial amount. Whereas local observations of <sup>3</sup>He have been obtained, this task appears to be much more difficult for D (Gloeckler and Geiss 1996). Recent estimates by Tarnopolski and Bzowski (2008) have shown that IBEX-Lo may be able to obtain direct D observations. Potential observations of H and D have substantial discovery potential, but their expected count rate is much more uncertain than the projected O observations because of the strong sensitivity of H and D flows in the inner heliosphere to the Sun's radiation pressure. Therefore, we will restrict the remainder of the discussion to O.

#### 4 IBEX Capabilities to Measure the Interstellar Gas Flow

The IBEX Mission has been implemented to focus on a single broad-scope scientific objective, the investigation of the global interaction of the heliosphere with the surrounding CHISM that occurs in the boundary regions. To achieve this goal experimentally, IBEX will take the first full-sky images of the heliospheric boundary in the "light" of energetic neutral

atoms (ENAs) in the energy range 10–6000 eV that emerge from the plasma and supra-thermal ion populations in the interaction processes at the termination shock and in the heliosheath (McComas et al. 2009, [this issue](#)). Of course, the flow of the pristine interstellar neutral gas and of their secondary products will be a natural part of these images, which will stand out because of their much higher directed fluxes. Because of the journey of these ENAs through the boundary regions into the inner heliosphere they are probes for the interaction in the outer heliosheath beyond the heliopause, thus addressing the fourth specific science question of the IBEX mission: What is the interstellar flow beyond the heliopause?

This section describes how the IBEX-Lo sensor will be used to probe the interstellar neutral gas flow distribution as it arrives at 1 AU.

#### 4.1 Influence of the IBEX Mission Design

To provide a series of full-sky images with ENAs, IBEX observations will be made with two large geometric factor single-pixel ENA cameras, which, in combination, cover the entire energy range with a comfortable overlap. These cameras are flown on a Sun-pointing spinning spacecraft in a high elliptical orbit around Earth. To keep the spin axis aligned with the Sun within  $\pm 4^\circ$ , the spacecraft is re-oriented so that it points  $\approx 4^\circ$  east of the Sun at the beginning of each orbit (with a period of about 8 days). After completion of the orbit the spin axis will point approximately  $4^\circ$  west of the Sun. The resulting IBEX viewing conditions are shown in Fig. 4 for two positions of the Earth on its orbit over the course of one year when the satellite is oriented such that the interstellar gas flow passes the field-of-view (FoV) of the IBEX-Lo sensor over a period of several weeks.

During a satellite spin, the sensors scan the angular flow distribution in ecliptic latitude. The two panels at the bottom of Fig. 4 show scans of the angular flow distribution in ecliptic longitude, as they would be accumulated by a spacecraft that keeps its spin axis exactly pointing at the Sun while following the Earth around the Sun. It is a combination of the changing orientation of the sensor FoV and the varying gravitational deflection of the flow along the Earth's orbit. Shown are the expected oxygen counts accumulated each day in an operation that keeps the IBEX-Lo sensor at the peak energy for each scan of the flow distribution, separately for the primary and secondary O component along with their combination. The latter is the actual observable in this measurement. As can be seen in Fig. 4, both combined distributions appear asymmetric. The asymmetry is due to the addition of the secondary component, which arrives at slightly larger deflection angles. The difference in deflection angle between these two components is shown as a function of ecliptic longitude, referenced to the inflow direction of the interstellar gas outside the heliosphere in Fig. 5. The angle difference is substantially larger in fall when compared with spring. This is due to the fact that in fall the observer is receding from the flow, while the observer is moving into flow in spring, following the Earth in its orbit. This behavior is also reflected in the overall much narrower angular distribution in spring. As will be discussed in connection with the sensor capabilities below, a smaller FoV will be employed to cope with the narrow distribution in spring. The width of the FoV must be significantly smaller (approximately by a factor of four) than the expected angular width of the distribution of about  $13^\circ$  FWHM (full width at half maximum) to avoid degradation of the asymmetry in the distribution (shown in the right hand panel of Fig. 4), which is key to the evaluation of the secondary neutral O component.

Taking the O flow distributions and demonstrating that they are asymmetric will satisfy the discovery level of the IBEX mission. However, to extract quantitative information on the interaction of the interstellar O with the heliospheric boundary at the exploration and the investigation level, the O distribution must be compared with the interstellar He distribution, which is unaffected by the interface. Ideally, the primary O distribution (shown in blue

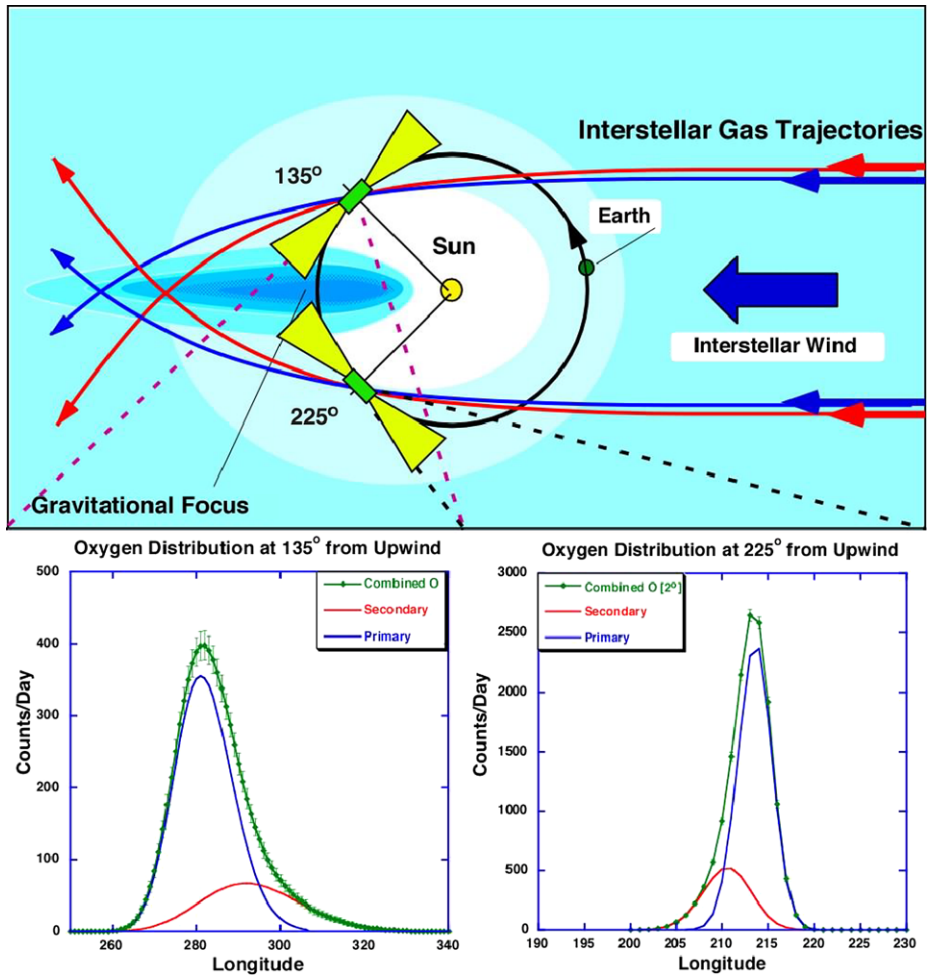
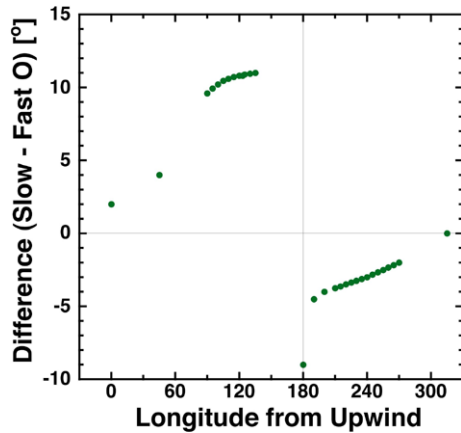


**Fig. 4** Schematic view of the interstellar gas flow through the inner heliosphere with the Earth's orbit and the IBEX-FoV for the two time periods of interstellar gas flow observations. The *insets* show the expected angular distributions of the gas flow with the primary and secondary components separate

in Fig. 4) should be subtracted from the combined distribution to reveal the unknown secondary O distribution. This can be achieved either by constructing the primary distribution from the accurately measured interstellar He flow based on observation with Ulysses GAS (Witte 2004) or by simultaneous observation of the He flow with IBEX-Lo. The former requires knowledge of the pointing of IBEX-Lo to better than  $\pm 0.2^\circ$  in absolute terms, i.e. the accuracy with which the He flow vector is known from the Ulysses observations; the latter requires a detection capability for He with IBEX-Lo in addition to observing O.

To facilitate accurate pointing of the IBEX-Lo sensor without undue impact on spacecraft resources and without setting stringent requirements on sensor pointing accuracy relative to the spacecraft attitude system, a small star sensor has been implemented as part of the IBEX-Lo sensor. By directly mounting the star sensor to the common baseplate of the IBEX-Lo sensor, which also holds the collimator, or the sole optical element, the impact of mechanical

**Fig. 5** Angle difference of the slow (secondary) O component relative to the fast (primary) O component as a function of ecliptic longitude relative to the interstellar upwind direction



alignment tolerances has been minimized. In pointing tests of the star sensor it has been established that the boresight of the IBEX-Lo collimator can be referenced in flight to stars in the star sensor FoV to  $\leq \pm 0.2^\circ$ . This capability will allow a direct comparison of IBEX flow vector measurements to those obtained by Ulysses GAS (Witte 2004) with the same accuracy as achieved with that instrument. A brief description of the star sensor and its calibration is provided in the paper by Fuselier et al. (2009, this issue).

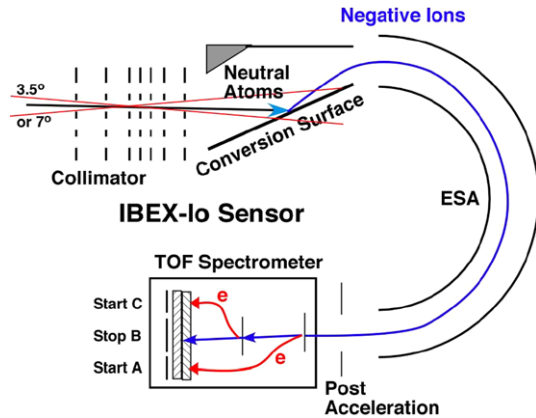
As will be discussed below, IBEX-Lo is indeed capable of observing simultaneously O and He neutral distributions. Therefore, a direct comparison of the interstellar O flow distribution, which is modified by the heliospheric interface, and that of He, which reflects the pristine CHISM conditions, will be performed with the same sensor. The precise absolute pointing capability provided by the star sensor will enable a triangulation of the He flow from different vantage points by combining the previous Ulysses observations and the future IBEX observations, with the prospects of improving the current knowledge.

#### 4.2 The IBEX-Lo Sensor

IBEX-Lo is one of the two large geometric factor single-pixel neutral atom cameras that together cover the energy range 10–6000 eV with considerable overlap from 250 to 2000 eV. Key requirements for both the IBEX-Lo and Hi cameras are large collecting power; excellent suppression of any unwanted background to unambiguously detect the low fluxes of the termination shock ENAs of  $5 \times 10^3$ – $1.5 \times 10^5 \text{ cm}^{-2} \text{ s}^{-1} \text{ sr}^{-1}$  in the energy range from 200 eV to 6 keV; and angular resolution of  $\leq 7^\circ$  FWHM (McComas et al. 2009, this issue).

IBEX-Lo is dedicated to the low energy portion from 10 to 2000 eV, and, because it covers the range of the interstellar flow components, it is outfitted as a mass spectrometer that can distinguish between H, He, and O. All requirements, functions, and implementation of the IBEX-Lo sensor are described in detail in the paper by Fuselier et al. (2009, this issue). Therefore, only the basic principles of the sensor and the characteristics most relevant to the interstellar flow observations will be presented here. Figure 6 shows a schematic cross-sectional view for one radial section of IBEX-Lo. The sensor is a large area single-pixel camera with a mechanical collimator as the key optical element, which accepts incoming neutral atoms within a solid angle FoV of  $\leq 7^\circ$  FWHM in its normal operational mode. To adequately observe the O flow distribution during the spring period when the angular

**Fig. 6** Schematic cross-sectional view of the IBEX-Lo sensor. In sequence incoming particles pass through a collimator, bounce off a neutral to negative ion conversion surface, pass an electrostatic analyzer, are post-accelerated, and then analyzed in a triple TOF system



distribution is about  $7^\circ$  in FWHM (see Fig. 4), IBEX-Lo has also been equipped with a high-resolution section of  $3.3^\circ$  FWHM angular acceptance that can be selected electrostatically by command. It is important to emphasize that the peak of a narrow flow distribution or its center of mass can be determined to much better accuracy than the angular resolution defined by the FoV, in this case to significantly better than  $1^\circ$ , mainly limited by counting statistics. Also, the mechanical collimator determines both the FoV and the pointing of the sensor, and the strong angular scattering at the conversion surface (CS) behind the collimator is largely irrelevant because (for the purpose of defining the angular acceptance) the CS is the detector element.

While bouncing off a CS a certain fraction of the neutrals become negative ions (Wurz 2000). The CS used is a highly polished Si wafer with a coating of tetrahedral amorphous carbon (ta-C) as described in Fuselier et al. (2009, this issue). This surface is inclined by  $15^\circ$  relative to the sensor boresight. The conversion is rather efficient for species that form stable negative ions, such as H, C, and O. However, it is rather inefficient for those that can only produce meta-stable negative ions, such as He. For the other noble gases a negative ion does not exist (Smirnov 1982). Also for N a stable negative ion does not exist (Hotop and Lineberger 1975), and the binding energies for the meta-stable negative N ion are so low (Mazeau et al. 1978) that useful negative ion yields are not expected for the IBEX investigation.

This behavior makes the CS a technique of choice for key neutral interstellar species, such as H and O, but it left the question open whether He could be detected directly with high enough efficiency. It should be pointed out that neutral atoms with energies above a few tens of eV will also release atoms that are present on the CS, of which a certain fraction take off as negative ions via sputtering and knock-on processes. For a relatively strong directional source of neutral atoms, such as the interstellar He flow at 1 AU, this process can serve as a valuable proxy for the direct detection of surface converted negative ions. In fact, this resembles the successful method used with the Ulysses GAS experiment (Witte 2004). GAS collects positive Li ions that are generated by the impact of incoming He atoms on a LiF surface. To evaluate how effective IBEX-Lo, with its diamond-like C conversion surface, is in the generation and collection of sputtered negative H, C, and O ions (from the diamond and always present water), and to find out whether a significant portion of negative He is produced, the sensor was also calibrated with a neutral He beam, as discussed below.

Negative ions are then collected electrostatically and guided through a toroidal electrostatic analyzer (ESA) with  $\approx 80\%$  energy resolution (right part of Fig. 6). For our purposes

this energy band choice allows a very effective collection of ions from the entire energy range of the interstellar flow distribution, while the analysis of the velocity distribution is left to the angular resolution of the entrance system and the gravitational deflection of the flow by the Sun, as described in Sect. 4.1. After post-acceleration by a voltage  $U_{\text{Acc}} = 16$  kV the ions are discriminated against remaining noise and background and analyzed for their mass in a triple time-of-flight (TOF) subsystem.

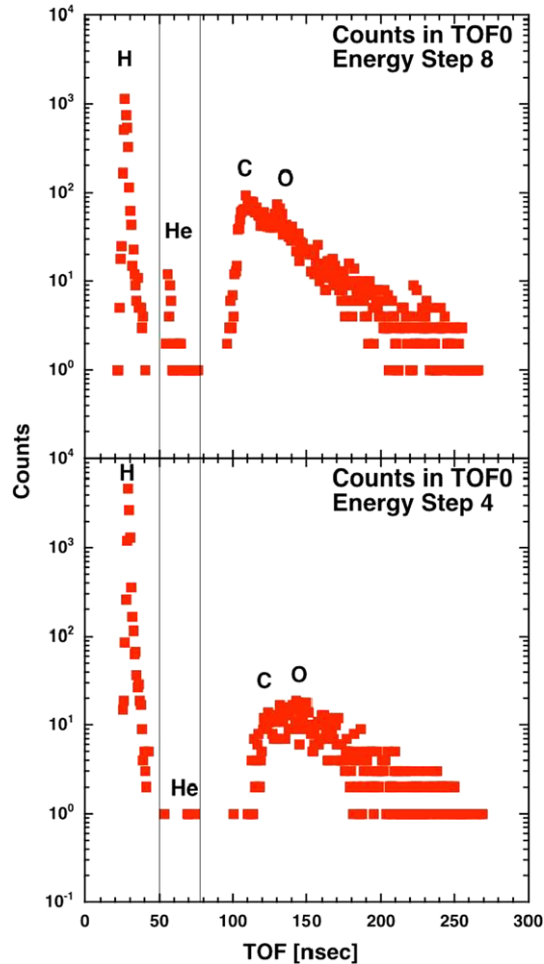
The TOF unit has been adapted from Cluster CODIF, similar sensors on FAST and Equator-S (Möbius et al. 1998b), and the more recent version STEREO PLASTIC (Galvin et al. 2007). Because of the extreme importance of background suppression for the IBEX mission, two similar TOF sections are used in series to achieve a genuine triple coincidence for the incoming ions (bottom left of Fig. 6). The incoming ions generate secondary electrons at the first carbon-foil that are guided to the outermost section of the micro-channel plate (MCP) detector. Similarly, electrons are generated at the second foil and guided to the innermost section of the MCP. The ions are detected in the center section, which is divided into 4 quadrants to allow for a separate background characterization. A single MCP pair is used. Three TOF values are determined between each of the foils and the MCP (TOF0 and TOF1) and between the two foils (TOF2). Each of these three TOF measurements is equivalent to the observation with a CODIF-like sensor. The ability to use any of the three measurements provides for very high efficiency. The quadrant position is derived from a delay line TOF measurement (TOF3). Ion detection with a maximum of background suppression is achieved when all 4 TOF signals are registered, but already a single TOF measurement provides adequate background suppression for the directed interstellar gas flow.

Combining the energy selected by the ESA  $E_{\text{ESA}}$  with the post-acceleration and the measured TOF  $\tau$  the species mass  $M$  is determined as follows:

$$M = 2(E_{\text{ESA}} + e \cdot U_{\text{Acc}}) \cdot \alpha \cdot \tau^2 / d^2, \quad (1)$$

where  $d$  is the length of the TOF unit and  $\alpha$  describes the reduction in energy due to losses in the entrance foils, which is energy and species dependent. This energy loss is determined during sensor calibration and in simulations. With a mass resolution  $M/\Delta M \geq 4$  as established during calibration, IBEX-Lo can unambiguously distinguish between H, He, and O and can even differentiate C and O contributions by fitting the respective TOF distributions of these two species. In its left half Fig. 7 shows a TOF spectrum taken during tests with IBEX-Lo using a neutral He beam. Shown are two TOF0 spectra, i.e. with the TOF measured between the first C-foil and the MCP, for which the separation between H and He is the largest, for energy step 8 (1500 eV incoming and detected particles; top) and for energy step 4 (130 eV particles, bottom). Shown are spectra compiled with only such events that contain all time-of-flight measurements, i.e. with the best noise and background suppression that the sensor offers. The peaks of H, He, and a combination of C and O are clearly separated, where a marked double-peak distribution also enables a quantitative separation of C and O in a two-peak fit. In step 8 converted He shows a peak that is clearly standing out (containing 53 events over the entire run). In step 4, at an energy commensurate with the interstellar He flow encountered by IBEX in spring, He counts are still seen, but with only 4 events the statistical significance for a positive identification of He is marginal. However, these measurements have established that  $\text{He}^-$  is indeed produced so that interstellar He may be directly identified with IBEX-Lo at 1 AU (Wurz et al. 2008). In addition, its presence can be inferred from the much more prominent sputtered products (H, C, and O). The H, C, and O present in the TOF spectra consists of negative ions created via sputtering and knock-off on the diamond-like carbon of the CS that typically contains a mono-layer

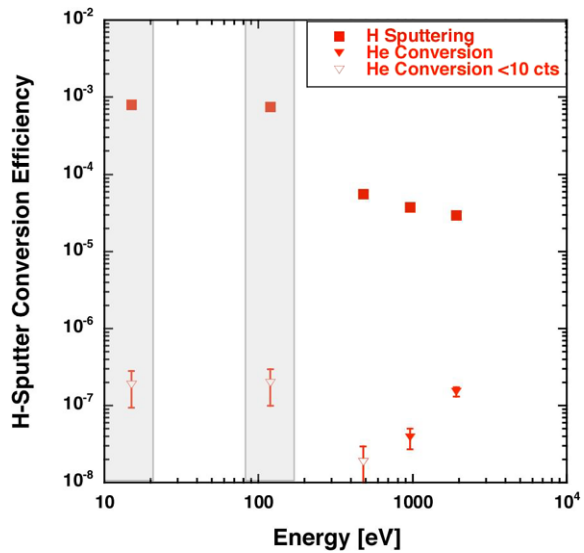
**Fig. 7** Time-of-flight spectra taken between the first C-foil and the MCP (TOF0, see Fig. 6) for a 1500 eV (top, Step 8) and 130 eV (bottom, Step 4 He beam (right)), taken for triple coincidence events. The TOF range for accepting He is indicated by the two vertical lines



of water. Hence the mass spectrum has the products of water and of carbon from the surface. The multi-species TOF spectra shown here also indicate that interstellar O is clearly distinguished from other species by IBEX-Lo. It should be noted here that the O flow will be detected at energies that are a factor of two, or two energy steps, above those of He. In the following we will see that sputtering leads to a very high yield so that the interstellar He flow can be observed with superb counting statistics in spring and in fall.

Figure 8 shows both the direct conversion efficiency of He and the efficiency for producing sputtered H as a function of energy over the entire energy range of IBEX-Lo, with the two semi-transparent rectangles indicating the energy ranges where interstellar He is observed in the spring and fall. For these energy ranges the combined sputter and sensor collection efficiency, which is relevant for the detection of incoming neutral atoms, is close to  $10^{-3}$ , i.e. only a factor of 20 below the combined conversion and collection efficiency for O, while the He flux density at 1 AU is approximately a factor of 1500 above that of O. Thus He will be observed with much more ease than O. The derived He conversion and collection efficiencies are much lower (by a factor of 5000), and it should be pointed out that at present only measurements with less than 10 events (4 triple events each that fall into

**Fig. 8** He conversion efficiency and efficiency for the combined production and collection of sputtered H versus energy. The two energy passbands relevant for interstellar He flow observations in spring (higher energy) and fall (lower energy) are highlighted. *Error bars* indicate statistical uncertainties of the measurements

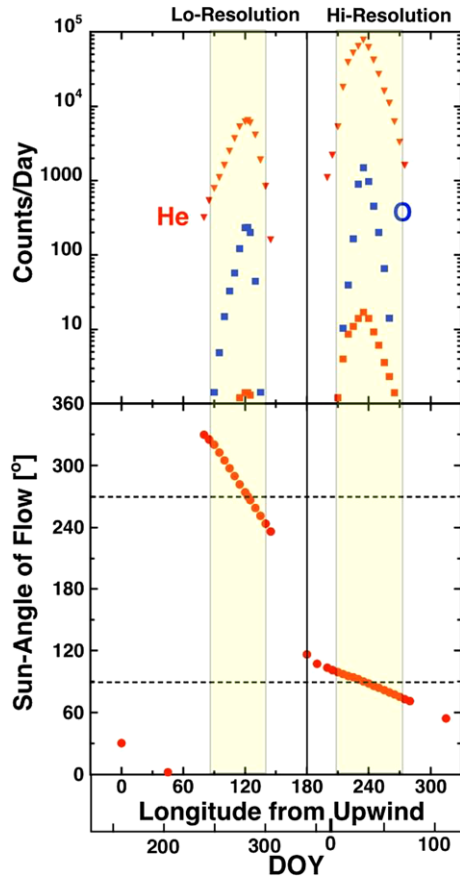


the He TOF range) have been collected. The error bars indicate the statistical uncertainty of each data point. With so few events (while absolutely excluding any background) it cannot be excluded that some events from the far tail of the H TOF distribution with orders of magnitude higher intensity contribute, and thus the final He conversion efficiency is even lower. For the purpose of this paper we are adopting the efficiency values shown here when we estimate the expected count rates for the detection of interstellar neutrals in spring and fall. It should be noted that the efficiency for the production of sputtered negative ions found in the energy range where the original He atoms arrive is surprisingly high. While the total yield of sputtered products is usually highest at energies significantly below the energy band of incoming neutral atoms, the yields shown here for the same energy band as the incoming particles produce rather high count rates as will be shown below. Using the energy steps of the incoming He atoms for the observation will avoid potential confusion with the possible collection of interstellar H atoms that will arrive with energies in the lowest energy step in spring. Also, this choice enables the potential direct detection of He through conversion, which will further validate the observation through sputtered particles.

## 5 Observation Campaign Planning

With the detection capability of IBEX-Lo for the key interstellar neutral species He and O clearly established in the sensor calibration, it remains the task of the IBEX mission planning to optimize a combined observation of the interstellar He and O flow distributions in the spring and fall when the bulk flow will be within the sensor FoV. Figure 9 shows expected accumulated counts per day for He and O in its upper panel and the direction of the flow relative to the Sun in the lower panel. The counts per day and the flow direction are plotted as a function of the position of the Earth (and thus IBEX) in ecliptic longitude, referenced to the upwind direction of the interstellar gas flow at large distances from the Sun. In the simulation, the geometric factors for the full collimator (lo-resolution) and the hi-resolution section only as established in the IBEX-Lo calibrations (Fuselier et al. 2009, [this issue](#)) were used to determine the expected count rates, and operation in the interstellar flow mode as

**Fig. 9** Expected number of counts/day integrated in spin direction for interstellar O (blue) and He (red) during the fall and spring passage of the flow with the IBEX-Lo FoV, with the sensor switched into its flow-sensing mode (top panel). Shown for He are the expected counts from surface conversion of He (squares) and those from sputtering of H off the surface (triangles), which are more abundant. Peak flow direction relative to the Sun as a function of ecliptic longitude (bottom panel). Both are shown as a function of ecliptic longitude from the interstellar medium upwind direction and day of the year (DOY) over two consecutive years. The two observation campaigns are highlighted



described below was assumed. In the representation in Fig. 9 we assumed for simplicity that the spin axis of the IBEX spacecraft would always point perfectly towards the Sun.

The viewing of both species is optimized and the necessary angular resolution of the directed flow measurement is achieved by switching into a flow sensing mode during two  $\approx 1.5$ -month periods in spring and fall. For  $\pm 30^\circ$  elevation above and below the ecliptic in the arrival direction of the flow, the electrostatic analyzer is set to the bulk flow energy of O for 7 steps and to that of He for 1 step of the 8 step energy cycle. In fall the regular collimator FoV of  $6.5^\circ$  FWHM is adequate to distinguish the pattern of the two O streams, but in spring the hi-resolution quadrant with a FoV of  $3.3^\circ$  FWHM is needed. In the spring, the remaining three quadrants with lo-resolution are switched off electrostatically at the CS. In this way the fact that the full collimator can be used for the broader angular distribution in fall compensates conveniently for the much lower neutral gas flux because the Earth recedes from the flow in the fall, while it moves into the ram direction in the spring. Figure 9 shows the number of counts per day collected for O and He (integrated in spin direction, when operated in this way) in the upper panel and the flow arrival direction relative to the Sun in the bottom panel.

The use of the interstellar gas flow mode leads to reduced coverage for the normal ENA H maps as a function of energy with IBEX-Lo for these observation periods. However, IBEX-Lo and IBEX-Hi have a substantial overlap in energy coverage from 250 eV to 2000 eV so

that IBEX-Hi still covers most of the energy range, and six months before and after each interstellar flow observation the same region of the sky is covered. Thus the interstellar flow mode operation only leads to reduced coverage for energies outside the energy band of the interstellar gas flow in its arrival directions in the sky. Here, the coverage of O, which arrives in the spacecraft rest frame at energies of 540 eV in the spring and 32 eV in the fall, is substantially increased by switching to the O flow energy for 7 out of 8 cycles. The remaining 8<sup>th</sup> cycle is used to collect a sample of the He flow for comparison with O.

As can be seen in the lower panel of Fig. 9, the peak of the gravitationally deflected interstellar flow distribution passes the sensor FoV at 90° and at 270° relative to the Sun from day of the year (DOY) 1 through 70 and from DOY 250 through 300 each year. The angle-scan results in the variation in the number of O and He atoms detected per day shown in the upper panel. The cut-off in the O viewing is used as the criterion for the two observation campaigns, which are indicated by the highlighted rectangles in Fig. 9. The campaigns will be run between January 5 and March 5 and between September 15 and October 25. In spring and in fall O and He will be seen with reasonable counting statistics. Because the sputtering efficiency is substantially higher than the direct conversion efficiency for He and the local flux at 1 AU is approximately 1500 times that of O, sputtered H, due to the impact of interstellar He, will be by far the strongest signal at 135 eV in spring and at 10 eV in fall. The count rates shown in Fig. 9 reflect the results from the IBEX-Lo calibration. The expected total number of interstellar O atoms will be  $\approx 2.2 \times 10^4$  in the spring and  $\approx 3400$  in the fall. Accounted for in the same way, the total of directly converted He atoms would potentially be  $\approx 470$  in the spring and only 40 in the fall, if the He conversion efficiencies shown in Fig. 6 do not contain events from the tail of the H distribution, which can be clearly assessed with observations that contain a better counting statistics than the available calibration measurements. Both the O and He conversion numbers are dwarfed, however, by the collection of sputtered H, with  $\approx 2.1 \times 10^6$  in the spring and  $\approx 3 \times 10^5$  in the fall. Both the converted He and the sputtered H will be collected simultaneously at the same energy setting for 135 eV in the spring and 10 eV in the fall, thus enabling a direct validation of the sputtered H as a product of the interstellar He. However, the huge number of sputtered particles from He will not result in additional background for the interstellar O, which is seen at 540 eV and 32 eV, respectively. Sputtering always creates products at energies lower than that of the incoming particles.

After the launch on October 19, 2008, the first spring passage of the interstellar flow falls into the time period when the first global ENA maps are taken with IBEX (McComas et al. 2009, [this issue](#)), for which a contiguous sky coverage with regular energy cycles and the full aperture of IBEX-Lo was anticipated. While the normal IBEX-Lo operation means visiting the peak energy of the interstellar O flow once every cycle of eight steps, the sensor geometric factor is now larger by a factor of 8.6, which more than compensates the duty cycle loss of a factor of 8. Using the entire collimator gains a factor of 4 in area and a somewhat higher transparency for the low-resolution section. Another factor of 2 is gained with the larger FoV angle in longitude, while a change in spin angle has no effect for a beam distribution when using integrated counts. Therefore, the total number of counts collected in this mode will be approximately the same for O and increased by a factor of 8.6 for He. Only the angular resolution of the measurement is not optimal for a quantitative evaluation of the O distribution whose angular half width is 13° in spring. Therefore, the normal operation mode will yield a first survey of the interstellar O and He flow distributions and at least yield an upper limit on the flow difference between the primary and secondary O streams.

In the anticipated operation scenario, IBEX will be in a high elliptical orbit with a typical orbital period of 8 days. At the beginning of each orbit the spin axis will be re-oriented to

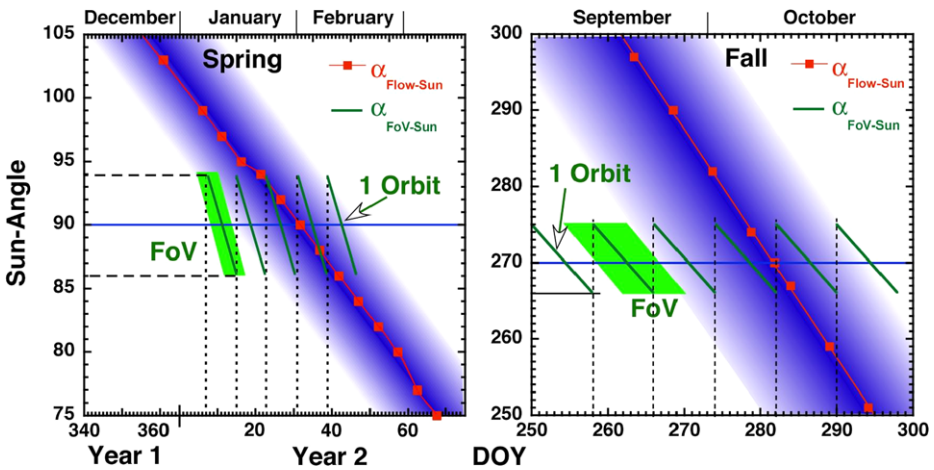


**Fig. 10** Variation of the CHISM flow arrival direction relative to the Sun (red line) along with indication of the angular distribution (blue shading) as a function of DOY. The change in the orientation of the FoV for a typical orbit with a period of 8 days is shown in green. (spring left and fall right)

about 4° behind or east of the Sun. Thus over the course of one orbit the FoV will drift across the direction 90° from the Sun until the spin axis points about 4° ahead or west of the Sun at the end of the orbit. At this point the spin axis will be reoriented so that it points again 4° east of the Sun. This behavior of the FoV is shown in Fig. 10 along with the change in the flow arrival direction for spring (left) and fall (right) as a function of the DOY. In spring this “ratcheting” motion of the FoV scans the full angular distribution over the course of several orbits with considerable overlap between two consecutive orbits, while in fall the drift of the FoV is almost parallel to the variation of the arrival direction. However, in fall the wider FoV is used and the distribution is wider. In this way the angular distribution of interstellar gas is still covered without gaps by consecutive FoV scans taking into account the FWHM of the FoV (green area in Fig. 10).

Figure 11 shows the resulting pattern of expected counts accumulated per day for O and He for the sputtered H counts over one pass of the interstellar flow distribution in spring. The periodicity of the shift of the spacecraft orientation with each orbit across the flow is clearly seen as a saw tooth pattern in the count rate. While this figure has been constructed from the simulation shown in Fig. 10 by transformation into the fixed orientation of the IBEX spacecraft for an entire orbit, the idealized observation can be reconstructed from the actual observations by reversing this step in the modeling. To compare model distributions of the interstellar flow with the observations both complete forward modeling up to the observations as simulated in Fig. 10 or reverse modeling of the observations into the expected interstellar flow distributions will be employed.

Making use of the spacecraft spin and timing information tagged onto each recorded particle, the flow distribution can also be evaluated in ecliptic latitude out of the ecliptic. Figure 12 shows the expected counts of interstellar O for the spring passage as shown in Figs. 10 and 11 in a color-coded 2-dimensional representation. The accumulated counts have been distributed by 6° pixels in latitude (commensurate with the 6° pixels of the all-sky ENA maps) and over 12 hours each to cover helio-longitude. The ratcheting of the FoV across the sky at the cadence of the spacecraft orbit is visible again in a similar pattern as in Fig. 11. The interstellar flow direction into  $-5.3^\circ$  in helio-latitude is evident from the offset

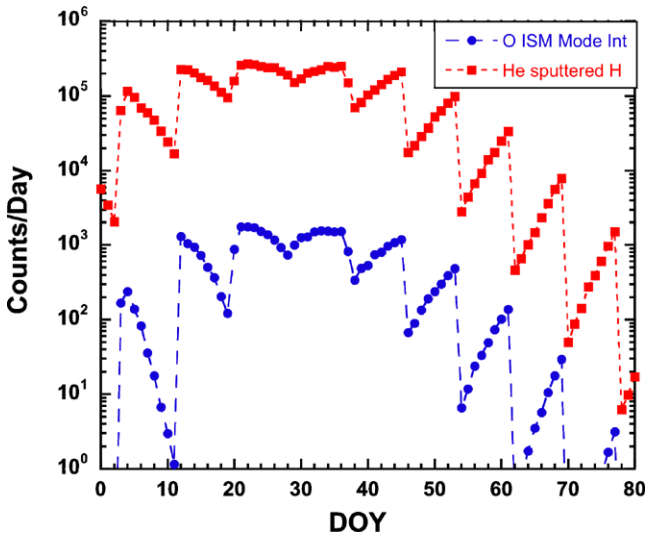
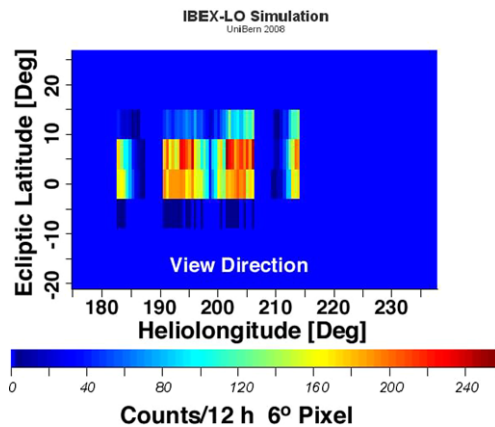


**Fig. 11** Simulation of expected counts accumulated per day for O and He over one pass of IBEX through the interstellar flow distribution in spring 2009. An eight-day orbit and re-orientation of the spin axis at the start of each orbit are assumed. Shown for He are the counts expected from sputtering of H off the CS

**Fig. 12** 2-dimensional view of the incoming interstellar O distribution in a color-coded representation. 6° pixels are shown in latitude, and a 12-hour cadence is chosen for the variation of the viewing direction relative to the peak of the flow distribution with spacecraft position in helio-longitude



of the maximum of counts in ecliptic latitude in Fig. 12. Because the timing of the incoming particles is recorded with an accuracy that is equivalent to better than 0.05°, the peak flow direction in latitude can be determined from the center of mass of the observed distribution with very high accuracy. It should be pointed out here that the expected deflection of the secondary neutrals due to the orientation of the interstellar magnetic field is mainly helio-latitude and thus can be identified in a deviation of the peak in the spin phase.

**6 Conclusions**

Interstellar neutral gas enters the inner heliosphere in the form of a wind due to the relative motion of the Sun. While the pristine He population enters the heliosphere unimpeded,

the charge exchange interaction with the interstellar plasma that is diverted around the heliopause produces a substantial secondary flow component for H and O with slower speed and higher temperature. Comparing the flow distributions of any of these two species with the undisturbed He flow will yield invaluable information to further constrain the interaction processes in the outer heliosheath and thus the ionization state in the surrounding CHISM. In addition, an interstellar magnetic field that is inclined relative to the interstellar gas flow vector distorts the shape of the heliosphere and as a consequence leads to a deflection of the secondary neutral gas flow component. Therefore, the combined velocity distributions of primary and secondary interstellar H and O entering the heliosphere are distinctly different from that of He. Any deflection of these flows relative to the pristine flow vector of the CHISM due to magnetic field effects becomes directly visible in ENA maps of these species as a deviation from the He flow vector. In comparison with 3-dimensional and time-dependent global heliospheric modeling, these observations will be used to further constrain the poorly known interstellar magnetic field strength and direction and to remove persisting ambiguities due to multiple causes of observed asymmetry effects in the heliosphere.

Close to the Sun the gas flow is subject to substantial gravitational deflection, which maps the original velocity distribution that is present at the termination shock into a related directional distribution. In turn, the velocity distributions can be obtained from directional distributions of interstellar neutrals.

By scanning through the angular distributions of interstellar neutrals with the single-pixel IBEX-Lo sensor, the Sun-pointed spinning IBEX satellite will obtain concurrent images of O and He in spring and fall when the deflected interstellar flow falls into the sensor FoV. Results from the calibration of the IBEX-Lo flight sensor demonstrate that the instrumentation will provide sufficient sensitivity and angular resolution for both O and He so that a direct comparison of the two different angular distributions becomes possible.

**Acknowledgements** The authors are grateful to the many individuals at the IBEX co-investigator institutions and the NASA Small Explorer Office who have made this program possible. Several of us (E.M., M.B., and V.I.) are indebted to the International Space Science Institute (ISSI) in Bern for the support of several workshops and scientific teams, which have helped the idea behind this paper from conception to implementation. This work is supported by NASA's Explorer Program under Grant NNG05EC85C, by NASA SR&T Grant NNG06GD55G, by the Swiss National Science Foundation, PRODEX, the Space Research Centre of the Polish Academy of Sciences, and the Russian Federation.

## References

- T.F. Adams, P.C. Frisch, *Astrophys. J.* **212**, 300 (1977)  
 W.I. Axford, in: *Solar Wind*. NASA SP-308, ed. by E.P. Sonnett, P.J. Coleman, J.M. Wilcox (1972), p. 609  
 M. Banaszekiewicz, M. Witte, H. Rosenbauer, *Astron. Astrophys. Suppl. Ser.* **120**, 587 (1996)  
 V.B. Baranov, Yu.G. Malama, *J. Geophys. Res.* **98**, 15157 (1993)  
 J.L. Bertaux, J.E. Blamont, *Astron. Astrophys.* **11**, 200 (1971)  
 J.L. Bertaux, R. Lallement, V.G. Kurt, E.N. Mironova, *Astron. Astrophys.* **150**, 1 (1985)  
 M. Bzowski, *Astron. Astrophys.* **483**, 1155 (2008)  
 M. Bzowski, E. Möbius, S. Tarnopolski, V. Izmodenov, G. Gloeckler, *Astron. Astrophys.* **491**, 7 (2008)  
 E. Chassefière, J.L. Bertaux, R. Lallement, V.G. Kurt, *Astron. Astrophys.* **160**, 229 (1986)  
 K.-P. Cheng, F.C. Bruhweiler, *Astrophys. J.* **364**, 573 (1990)  
 D.P. Cox, R.J. Reynolds, *Ann. Rev. Astron. Astrophys.* **25**, 303 (1987)  
 R.M. Crutcher, *Astrophys. J.* **254**, 82 (1982)  
 A.C. Cummings, E.C. Stone, C. Steenberg, *Astrophys. J.* **578**, 194 (2002)  
 H.J. Fahr, *Space Sci. Rev.* **15**, 483 (1974)  
 H.J. Fahr, G. Lay, C. Wulf-Mathies, *COSPAR Space Res.* **18**, 393 (1978)  
 H.J. Fahr, T. Kausch, H. Scherer, *Astron. Astrophys.* **357**, 268 (2000)  
 P.C. Frisch, *Nature* **293**, 377 (1981)

- P.C. Frisch, *Space Sci. Rev.* **72**, 499 (1995)
- P.C. Frisch, *Solar Journey: The Significance of our Galactic Environment for the Heliosphere and Earth*. Astrophysics and Space Science Library, vol. 338 (Springer, Berlin, 2006)
- P.C. Frisch et al., *Space Sci. Rev.* (2009, this issue)
- S. Fuselier et al., *Space Sci. Rev.* (2009, this issue)
- A.B. Galvin et al., *Space Sci. Rev.* (2007). doi:[10.1007/s11214-007-9296-x](https://doi.org/10.1007/s11214-007-9296-x)
- G. Gloeckler, J. Geiss, *Nature* **381**, 210 (1996)
- G. Gloeckler, L.A. Fisk, J. Geiss, *Nature* **386**, 374 (1997)
- G. Gloeckler, J. Geiss, *Space Sci. Rev.* **86**, 127 (1998)
- G. Gloeckler, J. Geiss, *Space Sci. Rev.* **97**, 169 (2001)
- T.E. Holzer, *Rev. Geophys. Space Phys.* **15**, 467 (1977)
- H. Hotop, W.C. Lineberger, *J. Phys. Chem. Ref. Data* **4**, 539 (1975)
- V.V. Izmodenov, *Space Sci. Rev.* **130**, 377 (2007)
- V.V. Izmodenov, Yu. Malama, R. Lallement, *Astron. Astrophys.* **317**, 193 (1997)
- V.V. Izmodenov, R. Kallenbach, eds., *The Physics of the Heliospheric Boundaries*, ISSI Scientific Report Series, vol. 5 (ESA, 2006). ISBN 1608-280X
- V.V. Izmodenov et al., *Astron. Astrophys.* **414**, L29 (2004)
- V.V. Izmodenov, D.B. Alexashov, A.V. Myasnikov, *Astron. Astrophys.* **437**, L35 (2005)
- V.V. Izmodenov, Y.G. Malama, M.S. Ruderman, *J. Adv. Space Res.* **41**, 318 (2008)
- J.R. Jokipii, *Space Sci. Rev.* **86**, 161 (1998)
- B. Klecker, *Space Sci. Rev.* **72**, 419 (1995)
- R. Lallement, P. Bertin, *Astron. Astrophys.* **266**, 79 (1992)
- R. Lallement, E. Quemerais, J.L. Bertaux et al., *Science* **307**, 1447 (2005)
- T.J. Linde, T.I. Gombosi, P.L. Roe, K.G. Powell, D.L. DeZeeuw, *J. Geophys. Res.* **103**, 1889 (1998)
- J.L. Linsky, *Space Sci. Rev.* **84**, 285 (1998)
- J.L. Linsky, A. Brown, Gayley et al., *Astrophys. J.* **402**, 694 (1993)
- Yu.G. Malama, V.V. Izmodenov, S.V. Chalov, *Astron. Astrophys.* **445**, 693 (2006)
- J. Mazeau, F. Grestau, R.I. Hall, A. Huetz, *J. Phys. B* **11**, L557 (1978)
- W. McClintock, R.C. Henry, J.L. Linsky, W.H. Moos, *Astrophys. J.* **225**, 465 (1978)
- D. McComas et al., *Space Sci. Rev.* (2009, this issue)
- E. Möbius, *Space Sci. Rev.* **143**, 465 (2009)
- E. Möbius, D. Hovestadt, B. Klecker et al., *Nature* **318**, 426 (1985)
- E. Möbius, D. Ruciński, D. Hovestadt, B. Klecker, *Astron. Astrophys.* **304**, 505 (1995)
- E. Möbius, D. Ruciński, M.A. Lee, P.A. Isenberg, *J. Geophys. Res.* **103**, 257 (1998a)
- E. Möbius et al., in: *Measurement Techniques in Space Plasmas*, ed. by R. Pfaff, J. Borowski, D. Young, Geophys. Monograph, vol. 102 (1998b), p. 243
- E. Möbius et al., *Astron. Astrophys.* **426**, 897 (2004)
- E. Möbius, M. Bzowski, H.-R. Müller, P. Wurz, in *Solar Journey: The Significance of our Galactic Environment for the Heliosphere and Earth*, ed. by P.C. Frisch (Springer, Berlin, 2006), pp. 209–258
- H.-R. Müller, G.P. Zank, *J. Geophys. Res.* **109**, A07104 (2004)
- H.-R. Müller, V. Florinski, J. Heerikhuisen et al., *Astron. Astrophys.* **491**, 43 (2008)
- D.J. Mullan, J.L. Linsky, *Astrophys. J.* **511**, 502 (1998)
- M. Opher, E.C. Stone, P.C. Liewer, *Astrophys. J.* **640**, L71 (2006)
- H.L. Pauls, G.P. Zank, L.L. Williams, *J. Geophys. Res.* **100**, 21595 (1995)
- N.V. Pogorelov, G.P. Zank, T. Ogino, *Astrophys. J.* **644**, 1299 (2006)
- N.V. Pogorelov, J. Heerikhuisen, G.P. Zank, *Astrophys. J.* **675**, L41 (2008)
- N. Prantzos, *Space Sci. Rev.* **84**, 225 (1998)
- E. Quémerais, J.L. Bertaux, R. Lallement et al., *J. Geophys. Res.* **104**, 12585 (1999)
- S. Redfield, *Space Sci. Rev.* (2008). doi:[10.1007/s11214-008-9422-4](https://doi.org/10.1007/s11214-008-9422-4)
- J.D. Richardson, Y. Liu, C. Wang, D.J. McComas, *Astron. Astrophys.* **491**, 1 (2008)
- J.D. Richardson, K.I. Paularena, A.J. Lazarus, J.W. Belcher, *Geophys. Res. Lett.* **22**, 1469 (1995)
- J. Slavin, P.C. Frisch, *Astrophys. J.* **565**, 364 (2002)
- B.M. Smirnov, *Negative Ions* (McGraw-Hill, New York, 1982)
- S. Tarnopolski, M. Bzowski, *Astron. Astrophys.* **483**, L35 (2008)
- G.E. Thomas, R.F. Krassa, *Astron. Astrophys.* **11**, 218 (1971)
- G.E. Thomas, *Ann. Rev. Earth Planet. Sci.* **6**, 173 (1978)
- H. Washimi, G.P. Zank, Q. Hu, T. Tanaka, in: *Turbulence and Non-Linear Processes in Astrophysical Plasmas*. AIP Conf. Proc., vol. 932 (2007), p. 153
- C.S. Weller, R.R. Meier, *Astrophys. J.* **193**, 471 (1974)
- M. Witte, *Astron. Astrophys.* **426**, 835 (2004)
- M. Witte, M. Banaszkiewicz, M. Rosenbauer, *Space Sci. Rev.* **78**, 289 (1996)

- B. Wolff, D. Koester, R. Lallement, *Astron. Astrophys.* **346**, 969 (1999)
- F.M. Wu, D.L. Judge, *Astrophys. J.* **231**, 594 (1979)
- P. Wurz, in *The Outer Heliosphere: Beyond the Planets*, ed. by K. Scherer, H. Fichtner, E. Marsch (Copernicus Gesellschaft e.V., Katlenburg-Lindau, 2000), p. 251
- P. Wurz, L. Saul, J. Scheer et al., *J. Appl. Phys.* **103** (2008). doi:[10.1063/1.2842398](https://doi.org/10.1063/1.2842398)
- G.P. Zank, *Space Sci. Rev.* **89**, 413 (1999)
- G.P. Zank, H.-R. Müller, *J. Geophys. Res.* **108**, 1240 (2003). doi:[10.1029/2002JA009689](https://doi.org/10.1029/2002JA009689)
- G.P. Zank, H.L. Pauls, L.L. Williams, D.T. Hall, *J. Geophys. Res.* **101**, 21639 (1996)
- G.P. Zank, H.-R. Müller, V. Florinski, P.C. Frisch, in *Solar Journey: The Significance of our Galactic Environment for the Heliosphere and Earth*, ed. by P.C. Frisch (Springer, Berlin, 2006), p. 23